PERGAMON

International Journal of Heat and Mass Transfer 45 (2002) 2777–2795

International Journal of HEAT and MASS TRANSFER

www.elsevier.com/locate/ijhmt

Conjugate free convection above a heated finite horizontal flat plate embedded in a porous medium

A.Z. Vaszi [a], L. Elliott [a,*], D.B. Ingham [a], I. Pop [b]

[a] *Department of Applied Mathematics, University of Leeds, Leeds LS2 9JT, UK*
[b] *Faculty of Mathematics, University of Cluj, CP 253, R-3400 Cluj, Romania*

Received 12 July 2001

Abstract

In this paper, we investigate the phenomenon of conjugate free convection in a semi-infinite porous medium above a heated finite plate. Numerical solutions of the full governing equations for the fluid region, coupled to the heat conduction equation in the finite plate, are obtained for a wide range of the non-dimensional parameters appearing in the problem, which are the Rayleigh number, Ra, the ratio of the thermal conductivities of the finite plate and the fluid, k, and the aspect ratio of the finite plate, λ, and a detailed description of the effects of these parameters on the characteristics of the fluid flow and the heat-transfer in the fluid is provided. For the high Rayleigh number regime, when a convective boundary-layer is assumed, the number of the non-dimensional parameters reduce to two and the results provided by this formulation show good agreement with the numerical results. In addition, for $Ra \gg 1$ a formulation which assumes one-dimensional heat conduction in the plate, is developed and provides computationally inexpensive results for the average conjugate boundary temperature and Nusselt number which compare well with the results obtained by the boundary-layer formulation.

Keywords: Natural convection; Conjugate; Boundary-layer; Horizontal; Finite plate; Porous medium; Numerical solutions

1. Introduction

Convective heat transfer in porous media has received a great deal of attention in recent years due to its importance in various technological applications such as geothermal systems, grain storage, fibre and granular insulation, cooling of electronic systems, packed-sphere beds, chemical catalytic reactors, groundwater hydrology, petroleum reservoirs, coal combustors, nuclear waste repositories and filtration, see books by Nakayama [1], Nield and Bejan [2], Ingham and Pop [3,4], Vafai [5] and Pop and Ingham [6].

Free convection boundary-layer flow in a porous medium above a heated horizontal surface, or below a cooled horizontal surface, was first considered by Cheng and Chang [7], who obtained similarity solutions of the governing equations. More recently, Merkin and Zhang [8], Higuera and Weidman [9] and Chandhary et al. [10] have published very detailed analytical and numerical solutions to this type of problem. In these studies cited, the surface was assumed to be of zero thickness and therefore any conduction in the wall was neglected. However, in many practical situations, especially those concerned with the design of thermal insulation, the conduction in the wall can have an important effect on the free convection flow adjacent to the surface. The conjugate free convection from either a vertical or a horizontal surface which is embedded in a porous medium has been central to a number of recent papers, e.g. Kimura et al. [11], Vynnycky and Kimura [12,13], Higuera and Weidman [9], Lesnic et al. [14], Pop and Merkin [15], Higuera [16] and Higuera and Pop [17]. An excellent review of this topic can be found in the review paper by Kimura et al. [18].

* Corresponding author. Tel.: +44-113-2335121; fax: +44-113-2335090.

E-mail addresses: lionel@amsta.leeds.ac.uk (L. Elliott), popi@math.ubbcluj.ro (I. Pop).

0017-9310/02/$ - see front matter
PII: S0017-9310(02)00002-9

Nomenclature

a	thickness of the plate
b	half longitudinal length of the plate
g	magnitude of the acceleration due to gravity
k_f	effective thermal conductivity of the convective fluid
k_s	thermal conductivity of the solid plate
k	ratio of the thermal conductivities in the solid plate and the fluid
K	permeability of the isotropic porous medium
Nu	local Nusselt number
$\overline{Nu}$	average Nusselt number
Ra	Rayleigh number, $Ra = \frac{gK\beta(T_c - T_\infty)b}{\alpha\nu}$
T_c	constant temperature at the bottom surface of the solid plate
T_∞	temperature at infinity
u, v	fluid velocity components in the x and y directions, respectively
$\overline{u}_b$	non-dimensional average fluid velocity on the conjugate boundary
x, y	horizontal and vertical Cartesian coordinate, respectively
X	shifted x coordinate, $x + 1$
Y	transformed y coordinate, $Ra^{1/3}y$
α	effective thermal diffusivity of the porous medium
β	coefficient of the thermal expansion
ζ	similarity variable, $Y/X^{2/3}$
$\hat{\zeta}$	transformed ζ variable, $\theta_0^{1/3}\zeta$
θ_f	non-dimensional temperature in the fluid medium
θ_s	non-dimensional temperature in the solid plate
θ_b	non-dimensional conjugate boundary temperature
$\overline{\theta}_b$	non-dimensional average conjugate boundary temperature
λ	aspect ratio of the solid plate
ν	kinematic viscosity of the fluid
ξ, η	elliptical coordinates
$\hat{\xi}$	transformed x or X coordinate, $1 - (1 - x)^{2/3}$ or $X^{2/3}$
ψ	streamfunction

The most comprehensive analytical and numerical investigations of such problems are those of Vynnycky and Kimura [12,13]. They obtained computational solutions to the governing heat and momentum (Darcy) equations when both the longitudinal and transverse conduction effects in the wall were present for the problems of free convection due to a heated vertical plate in both the steady and the transient case. The horizontal configuration for the free convection in a porous medium near an upward facing cooled (or a downward facing heated) plate which has a finite length was investigated by Kimura et al. [11] and Higuera and Weidman [9] when the plate has zero thickness.

In this paper, we examine the problem of conjugate free convection heat transfer from an upward facing heated (or a downward facing cooled) finite plate which has a non-zero thickness, and is adjacent to a semi-infinite porous medium when both the longitudinal and transverse conduction effects in the plate are present. First, we provide a mathematical formulation for the full problem, identifying the relevant non-dimensional parameters, namely, the Rayleigh number, Ra, the thermal conduction ratio between the solid and the porous medium, k, and the plate aspect ratio between the thickness of the plate and half the longitudinal length of the plate, λ. The high Rayleigh number regime is treated in two ways: first, by coupling the boundary-layer flow within the porous medium to the two-dimensional conduction within the plate and solving the resulting problem numerically, and second, by performing a one-dimensional averaging process over the length of the plate to obtain the average conjugate boundary temperature and mean Nusselt number. The full equations are then solved numerically by finite-difference techniques using a transformation from Cartesian to elliptic coordinates for the fluid-saturated porous medium region. This scheme is both accurate and robust and has recently been used successfully for similar problems, see Vynnycky and Kimura [19], Vynnycky and Pop [20] and Vynnycky et al. [21]. We have compared the solutions obtained by the different solution procedures over a wide range of the values of the parameters involved.

2. Governing equations

The configuration of the problem under consideration is schematically shown in Fig. 1. A horizontal plate has a thickness a, and it is made up of three parts, namely, a plate of finite length $2b$ and two thermally insulating, semi-infinite plates, which are each attached to the opposite ends of the finite plate to produce a single infinite non-homogeneous horizontal plate. The bottom surface of the finite plate is held at a fixed temperature T_c. We are interested in the temperature within the finite plate and above the plate, where there is a porous medium which is at a uniform ambient temperature, T_∞, far from the plate, where $T_c > T_\infty$ and it is also assumed that the porous medium is isotropic and homogeneous.

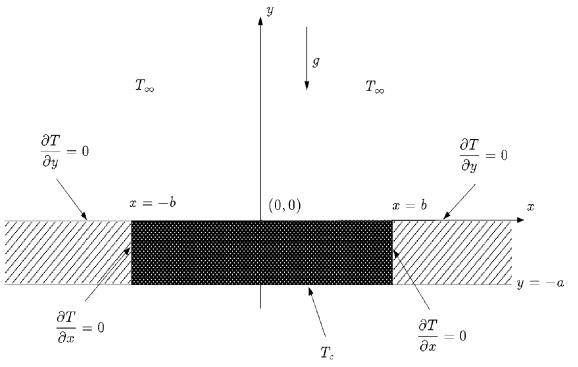

Fig. 1. Physical configuration.

The two-dimensional steady-state equations of the Darcy flow model, namely, the mass, momentum and energy conservation laws are (see Nield and Bejan [2])

$$\frac{\partial u}{\partial x}+\frac{\partial v}{\partial y}=0, \tag{1}$$

$$\frac{\partial u}{\partial y}-\frac{\partial v}{\partial x}=-\frac{gK\beta}{v}\frac{\partial T_{\mathrm{f}}}{\partial x} \tag{2}$$

and

$$u\frac{\partial T_{\mathrm{f}}}{\partial x}+v\frac{\partial T_{\mathrm{f}}}{\partial y}=\alpha\left(\frac{\partial^2 T_{\mathrm{f}}}{\partial x^2}+\frac{\partial^2 T_{\mathrm{f}}}{\partial y^2}\right), \tag{3}$$

where u, v are the fluid velocity components in the x, y directions, respectively, g is the gravitational acceleration, K is the permeability of the isotropic porous medium, β is the coefficient of thermal expansion, v is the kinematic viscosity of the fluid, T_{f} is the temperature of the fluid-saturated porous medium and α is the effective thermal diffusivity of the porous medium. In order to effect the coupling between the fluid flow and the fluid temperature fields, the Oberbeck–Boussinesq approximation has been employed by introducing the coefficient of thermal expansion β in the buoyancy term in Eq. (2).

The heat transfer in the solid plate is described by the steady-state heat conduction equation,

$$\frac{\partial^2 T_{\mathrm{s}}}{\partial x^2}+\frac{\partial^2 T_{\mathrm{s}}}{\partial y^2}=0, \tag{4}$$

where T_{s} denotes the temperature in the solid plate, and the boundary conditions on the plate may now be expressed as follows:

$$\psi=0 \quad \text{on } y=0,\ -\infty<x<\infty, \tag{5a}$$

$$T_f=T_{\mathrm{s}} \quad \text{on } y=0,\ |x|\leqslant b, \tag{5b}$$

$$k_{\mathrm{f}}\frac{\partial T_{\mathrm{f}}}{\partial y}=k_{\mathrm{s}}\frac{\partial T_{\mathrm{s}}}{\partial y} \quad \text{on } y=0,\ |x|\leqslant b, \tag{5c}$$

$$\frac{\partial T_{\mathrm{f}}}{\partial y}=0 \quad \text{on } y=0,\ |x|>b, \tag{5d}$$

$$T_{\mathrm{s}}=T_{\mathrm{c}} \quad \text{on } y=-a,\ |x|\leqslant b, \tag{5e}$$

$$\frac{\partial T_{\mathrm{s}}}{\partial x}=0 \quad \text{on } x=\pm b,\ -a\leqslant y\leqslant 0, \tag{5f}$$

where k_{f} and k_{s} denote the thermal conductivities of the fluid and of the solid plate, respectively, and the stream-function ψ is defined such that the continuity equation (1) is satisfied identically, thus $u=\partial\psi/\partial y$ and $v=-\partial\psi/\mathrm{d}x$.

The boundary conditions at large distances from the finite heated plate are

$$v\to 0,\ T_{\mathrm{f}}\to T_\infty \quad \text{as } x\to\pm\infty,\ y\geqslant 0, \tag{6a}$$

$$u\to 0,\ T_{\mathrm{f}}\to T_\infty \quad \text{as } y\to\infty,\ -\infty<x<\infty. \tag{6b}$$

By introducing the non-dimensional variables

$$\hat{x}=\frac{x}{b},\quad \hat{y}=\frac{y}{b},\quad \hat{\psi}=\frac{\psi}{\alpha},\quad \hat{\theta}_f=\frac{T_f-T_\infty}{T_c-T_\infty},$$
$$\hat{\theta}_s=\frac{T_s-T_\infty}{T_c-T_\infty} \tag{7}$$

and subsequently, on dropping the hats for convenience, Eqs. (2)–(4) become

$$\frac{\partial^2\psi}{\partial x^2}+\frac{\partial^2\psi}{\partial y^2}=-Ra\frac{\partial\theta_{\mathrm{f}}}{\partial x}, \tag{8a}$$

$$\frac{\partial^2\theta_{\mathrm{f}}}{\partial x^2}+\frac{\partial^2\theta_{\mathrm{f}}}{\partial y^2}=\frac{\partial\psi}{\partial y}\frac{\partial\theta_{\mathrm{f}}}{\partial x}-\frac{\partial\psi}{\partial x}\frac{\partial\theta_{\mathrm{f}}}{\partial y}, \tag{8b}$$

$$\frac{\partial^2\theta_{\mathrm{s}}}{\partial x^2}+\frac{\partial^2\theta_{\mathrm{s}}}{\partial y^2}=0, \tag{8c}$$

where the Rayleigh number is defined by $Ra=(gK\beta(T_{\mathrm{c}}-T_\infty)b)/\alpha v$, whilst the boundary conditions (5a)–(5f), and (6a) and (6b) in their non-dimensional form become

$$\psi=0 \quad \text{on } y=0,\ -\infty<x<\infty, \tag{9a}$$

$$\theta_{\mathrm{f}}=\theta_{\mathrm{s}} \quad \text{on } y=0,\ |x|\leqslant 1, \tag{9b}$$

$$\frac{\partial\theta_f}{\partial y}=k\frac{\partial\theta_{\mathrm{s}}}{\partial y} \quad \text{on } y=0,\ |x|\leqslant 1, \tag{9c}$$

$$\frac{\partial\theta_{\mathrm{f}}}{\partial y}=0 \quad \text{on } y=0,\ |x|>1, \tag{9d}$$

$$\theta_{\mathrm{s}}=1 \quad \text{on } y=-\lambda,\ |x|\leqslant 1, \tag{9e}$$

$$\frac{\partial\theta_{\mathrm{s}}}{\partial x}=0 \quad \text{on } x=\pm 1,\ -\lambda\leqslant y\leqslant 0 \tag{9f}$$

and

$$\frac{\partial\psi}{\partial x}\to 0,\ \theta_{\mathrm{f}}\to 0 \quad \text{as } x\to\pm\infty,\ y\geqslant 0, \tag{10a}$$

$$\frac{\partial\psi}{\partial y}\to 0,\quad \theta_f\to 0\quad \text{as } y\to\infty,\quad -\infty<x<\infty, \tag{10b}$$

where $\lambda=a/b$ and $k=k_s/k_f$ denote the aspect ratio of the conducting plate and the ratio of the thermal conductivities in the solid plate and the fluid, respectively.

3. Mathematical formulation for $Ra\gg 1$

When the Rayleigh number is very large then both viscous and thermal boundary layers, starting at the locations $(-1,0)$ and $(1,0)$, develop above the plate, with each boundary-layer mathematically unaware of the existence of the other. Thus the boundary layers collide on $x=0$, and therefore the solutions are invalid in the vicinity of the origin. If we let the non-dimensional temperature at the locations $(-1,0)$ and (1,0) be denoted by θ_0, $0\leqslant\theta_0\leqslant 1$, then there are two possible situations which may occur in the analysis, namely $0<\theta_0\leqslant 1$ or $\theta_0=0$.

As indicated in Nield and Bejan [2], in the boundary-layer the normal component of the fluid velocity, v, is small compared with the tangential fluid velocity component, u, and derivatives with respect to y of a quantity, such as the fluid velocity and temperature, are large compared with the derivatives of that quantity with respect to x, and accordingly the terms $\partial^2\psi/\mathrm{d}x^2$ and $\partial^2\theta_f/\partial x^2$ can be omitted from Eqs. (8a) and (8b). Scaling the quantities ψ and y, and maintaining the balance in these equations, indicates that the appropriate scalings are

$$\psi=Ra^{1/3}\Psi,\quad y=Ra^{-1/3}Y. \tag{11}$$

Concentrating on the boundary-layer which develops from the point $(-1,0)$, and using the transformation $x=X-1$ such that the analysis applies to the left half-side of the physical domain, the transformed equations become

$$\frac{\partial^2\Psi}{\partial Y^2}=-\frac{\partial\theta_f}{\partial X}, \tag{12a}$$

$$\frac{\partial^2\theta_f}{\partial Y^2}=\frac{\partial\Psi}{\partial Y}\frac{\partial\theta_f}{\partial X}-\frac{\partial\Psi}{\partial X}\frac{\partial\theta_f}{\partial Y} \tag{12b}$$

and have to be solved subject to the boundary conditions (9a)–(9f), and (10a) and (10b) which become

$$\Psi=0\quad \text{on } Y=0,\ 0\leqslant X\leqslant 1, \tag{13a}$$

$$\theta_s=\theta_f\quad \text{on } Y=0,\ 0\leqslant X\leqslant 1, \tag{13b}$$

$$\frac{\partial\theta_s}{\partial y}=\sigma\frac{\partial\theta_f}{\partial Y}\quad \text{on } Y=0,\ 0\leqslant X\leqslant 1, \tag{13c}$$

$$\frac{\partial\Psi}{\partial Y}\to 0,\quad \theta_f\to 0\ \text{as } Y\to\infty, \tag{13d}$$

where the parameter σ is given by $\sigma=Ra^{1/3}/k$. Further, since fluid only flows into the boundary-layer, we have only used the inflow boundary conditions for $Y\to\infty$. In addition, we require boundary conditions at $X=0$, and since we have assumed that the boundary-layer originates at $X=0$, the flow has been taken to be at rest for $X\leqslant 0$, thus the boundary conditions at $X=0$ are the following:

$$\Psi=\frac{\partial\Psi}{\partial X}=0\quad \text{at } X=0. \tag{14}$$

Case $0<\theta_0\leqslant 1$. For the purpose of the analytical development and the ultimate numerical solution when $0<\theta_0\leqslant 1$, we reformulate Eqs. (12a)–(14), using the similarity variables as introduced by Cheng and Chang [7] for the standard free convection problem of a constant wall temperature. On writing

$$\Psi(X,Y)=X^{1/3}F(X,\zeta),\quad \theta_f(X,Y)=G(X,\zeta),$$
$$\zeta=Y/X^{2/3}, \tag{15}$$

Eqs. (12a), (12b) reduce to

$$F''-\frac{2}{3}\zeta G'=-X\frac{\partial G}{\partial X}, \tag{16a}$$

$$G''+\frac{1}{3}FG'=X\left(F'\frac{\partial G}{\partial X}-G'\frac{\partial F}{\partial X}\right), \tag{16b}$$

where the primes denote differentiation with respect to ζ. Further, the boundary conditions (13a),(13b),(13c) and (13d) for $0\leqslant X\leqslant 1$ in terms of F and G are given by

$$F=0,\quad \theta_s=G,\quad \frac{\partial\theta_s}{\partial y}=\frac{\sigma}{X^{2/3}}G'\quad \text{on } \zeta=0, \tag{17a}$$

$$F'\to 0,\quad G\to 0\quad \text{as } \zeta\to\infty \tag{17b}$$

with Eq. (14) automatically satisfied by the choice of the similarity variables.

Having two conditions which connect the temperature variables for the fluid and for the solid on the conjugate boundary, we use the second boundary condition from (17a) for solving the equations in the fluid, whilst the third boundary condition from (17a) is used for solving the equations in the solid.

On letting $X\to 0$, we obtain the following ordinary differential equations:

$$F''-\frac{2}{3}\zeta G'=0,\quad G''+\frac{1}{3}FG'=0, \tag{18}$$

with the boundary conditions

$$F=0,\quad G=\theta_0\ \text{on } \zeta=0\quad F'\to 0,$$
$$G\to 0\ \text{as } \zeta\to\infty \tag{19}$$

and these equations, together with their boundary conditions, constitute the initial conditions for the equations for the fluid region.

The constant θ_0 is as yet unknown and it is calculated as part of the solution procedure when solving the coupled equations for the fluid and the solid and in order to remove θ_0 from Eqs. (18) and (19), we make the canonical substitutions

$$F(X,\zeta)=\theta_0^{1/3}\hat{F}(X,\hat{\zeta}),\quad G(X,\zeta)=\theta_0\hat{G}(X,\hat{\zeta}),$$
$$\zeta=\theta_0^{-1/3}\hat{\zeta}, \tag{20}$$

which leave Eqs. (16a)–(19) unaltered, except for the second and third boundary condition of (17a) and the second boundary condition of (19). Thus the second boundary condition of (17a) and that of (19) become $\hat{G}=\theta_s/\theta_0$ and $\hat{G}=1$ on $\hat{\zeta}=0$.

The third boundary condition of (17a) which is employed in the heat conduction equation for the plate region, after applying the substitutions (20), takes the form

$$\frac{\partial\theta_s}{\partial y}=\frac{\sigma}{X^{2/3}}\theta_0^{4/3}\hat{G}' \quad \text{on } \hat{\zeta}=0. \tag{21}$$

In order to remove the singular behaviour of this expression in the vicinity of $X=0$, we introduce plane polar coordinates (r,ϕ), which are given by $X=r\cos\phi$, $y=r\sin\phi$. Thus the boundary condition (9f) at $X=0$ becomes

$$\frac{\partial\theta_s}{\partial\phi}=0 \quad \text{on } \phi=-\frac{\pi}{2}, \tag{22a}$$

whilst the boundary condition (21), in the vicinity of $X=0$, is given by

$$\frac{\partial\theta_s}{\partial\phi}=\sigma\theta_0^{4/3}\hat{G}'(0,0)r^{1/3} \quad \text{on } \phi=0, \tag{22b}$$

where it should be noted that $\hat{G}'(0,0)$ is a constant which can be obtained as $G'(0,0)$ from the solution of Eqs. (18) subject to the boundary conditions (19), except that the boundary condition $G=\theta_0$ is now $G=1$ on $\zeta=0$.

The Eq. (8c), in terms of (X,y), along with the boundary conditions (22a) and (22b) has the following solution:

$$\hat{\theta}_s(r,\phi)=6\sigma\theta_0^{4/3}\hat{G}'(0,0)r^{1/3}\sin\left(\frac{\phi-\pi}{3}\right) \tag{23}$$

and using this solution we may remove the singularity at $r=0$ by writing $\theta_s=\hat{\theta}_s+\theta_s^{\star}$. Thus $\theta_s^{\star}$ satisfies the equation

$$\frac{\partial^2\theta_s^{\star}}{\partial X^2}+\frac{\partial^2\theta_s^{\star}}{\partial y^2}=0 \tag{24}$$

and the boundary conditions (9c), (9e) and (9f) are now given by

$$\frac{\partial\theta_s^{\star}}{\partial y}=\frac{\sigma\theta_0^{4/3}}{X^{2/3}}\hat{G}'-\frac{\partial\hat{\theta}_s}{\partial y} \quad \text{on } y=0,\ 0\leqslant X\leqslant 1, \tag{25a}$$

$$\theta_s^{\star}=1-\hat{\theta}_s \quad \text{on } y=-\lambda,\ 0\leqslant X\leqslant 1, \tag{25b}$$

$$\frac{\partial\theta_s^{\star}}{\partial X}=0 \quad \text{on } X=0,\ -\lambda\leqslant y\leqslant 0, \tag{25c}$$

$$\frac{\partial\theta_s^{\star}}{\partial X}=-\frac{\partial\hat{\theta}_s}{\partial X} \quad \text{on } X=1,\ -\lambda\leqslant y\leqslant 0, \tag{25d}$$

where on the axis of symmetry $X=1$ the boundary condition (25d) has been introduced for the equation in the solid.

Since the heating is most intense close to $X=0$, in order to acquire a more accurate solution to the equations in the plate then a refinement was made in the X direction by introducing the variable $\hat{\xi}$ given by $\hat{\xi}=X^{2/3}$. Thus Eq. (24) for the plate region in the $(\hat{\xi},y)$ co-ordinate system is given by

$$\frac{4}{9}\hat{\xi}\frac{\partial^2\theta_s^{\star}}{\partial\hat{\xi}^2}-\frac{2}{9}\frac{\partial\theta_s^{\star}}{\partial\hat{\xi}}+\hat{\xi}^2\frac{\partial^2\theta_s^{\star}}{\partial y^2}=0, \tag{26}$$

whilst the boundary conditions (25a)–(25d), using the expressions (23) and the results for $\partial\hat{\theta}_s/\partial y$ and $\partial\hat{\theta}_s/\partial X$, can be written in the following form:

$$\frac{\partial\theta_s^{\star}}{\partial y}=\frac{A}{\hat{\xi}}\left[\frac{\hat{G}'(\hat{\xi}^{3/2},0)}{\hat{G}'(0,0)}-1\right] \text{on } y=0,\quad 0<\hat{\xi}\leqslant 1, \tag{27a}$$

$$\theta_s^{\star}=1-6A(\hat{\xi}^3+\lambda^2)^{1/6}\sin\left[\frac{\arctan(-\lambda/\hat{\xi}^{3/2})-\pi}{3}\right]$$
$$\text{on } y=-\lambda,\ 0\leqslant\hat{\xi}\leqslant 1, \tag{27b}$$

$$\frac{\partial\theta_s^{\star}}{\partial\hat{\xi}}=0 \quad \text{on } \hat{\xi}=0,\ -\lambda\leqslant y\leqslant 0, \tag{27c}$$

$$\frac{\partial\theta_s^{\star}}{\partial\hat{\xi}}=\frac{3A}{(1+y^2)^{1/3}}\sin\left[\frac{2\arctan y+\pi}{3}\right]$$
$$\text{on } \hat{\xi}=1,\ -\lambda\leqslant y\leqslant 0, \tag{27d}$$

where $A=\sigma\theta_0^{4/3}\hat{G}'(0,0)$.

Case $\theta_0=0$. We now consider the solution of Eqs. (12a) and (12b) assuming that $\theta_0=0$. On looking for the appropriate scaling of the boundary-layer near $X=0$, we obtain the following similarity transformations:

$$\Psi(X,Y)=X^{1/2}F(X,\zeta),$$
$$\theta_f(X,Y)=X^{1/2}G(X,\zeta),\ \ \zeta=Y/X^{1/2} \tag{28}$$

and on applying these transformations, Eqs. (12a) and (12b) for the fluid region become

$$F''-\frac{1}{2}\zeta G'+\frac{1}{2}G=-X\frac{\partial G}{\partial X}, \tag{29a}$$

$$G''+\frac{1}{2}(FG'-F'G)=X\left(F'\frac{\partial G}{\partial X}-G'\frac{\partial F}{\partial X}\right). \tag{29b}$$

The boundary conditions (13a)–(13d) for $0 \leqslant X \leqslant 1$ are now given by

$$F = 0, \quad G' = \frac{1}{\sigma}\frac{\partial \theta_s}{\partial y} \text{ on } \zeta = 0, \tag{30a}$$

$$F' \to 0, \quad G \to 0 \text{ as } \zeta \to \infty, \tag{30b}$$

where Eq. (13b) has been omitted to be used in the equations for the plate region. Further, Eq. (14) is automatically satisfied by the choice of the similarity variables (28).

On letting $X \to 0$, we obtain the system of ordinary differential equations

$$F'' - \frac{1}{2}\zeta G' + \frac{1}{2}G = 0, \quad G'' + \frac{1}{2}(FG' - F'G) = 0, \tag{31}$$

which have to be solved subject to the boundary conditions (30a) and (30b), and their solution provides the initial conditions for the equations in the fluid region.

This time there is no singularity near the origin with respect to θ_s that satisfies Eq. (8c) (now given in (X, y) coordinates) subject to the boundary conditions (9b), (9e) and (9f), which now become

$$\theta_s = X^{1/2}G \quad \text{on } y = 0, \ 0 \leqslant X \leqslant 1, \tag{32a}$$

$$\theta_s = 1 \quad \text{on } y = -\lambda, \ 0 \leqslant X \leqslant 1, \tag{32b}$$

$$\frac{\partial \theta_s}{\partial X} = 0 \quad \text{on } X = 0, \ -\lambda \leqslant y \leqslant 0, \tag{32c}$$

$$\frac{\partial \theta_s}{\partial X} = 0 \quad \text{on } X = 1, \ -\lambda \leqslant y \leqslant 0, \tag{32d}$$

where it should be noted that the boundary condition (32d) has been introduced as a symmetry condition on the central vertical line of the plate.

As in the $0 < \theta_0 \leqslant 1$ case, we introduce the variable $\hat{\xi}$ and then Eq. (24) for the plate region (with θ_s replacing $\theta_s^{\star}$) becomes Eq. (26) (again, with θ_s replacing $\theta_s^{\star}$), whilst the boundary conditions (32a)–(32d) become

$$\theta_s = \hat{\xi}^{3/4}G, \quad \text{on } y = 0, \ 0 \leqslant \hat{\xi} \leqslant 1, \tag{33a}$$

$$\theta_s = 1 \quad \text{on } y = -\lambda, \ 0 \leqslant \hat{\xi} \leqslant 1, \tag{33b}$$

$$\frac{\partial \theta_s}{\partial \hat{\xi}} = 0 \quad \text{on } \hat{\xi} = 0, \ -\lambda \leqslant y \leqslant 0, \tag{33c}$$

$$\frac{\partial \theta_s}{\partial \hat{\xi}} = 0 \quad \text{on } \hat{\xi} = 1, \ -\lambda \leqslant y \leqslant 0. \tag{33d}$$

Approximate one-dimensional solution for $0 < \theta_0 \leqslant 1$. In order to estimate the average conjugate boundary temperature, $\overline{\theta}_b$, and the average Nusselt number, $\overline{Nu}$, in the situation when $Ra \gg 1$, we have developed an approximate one-dimensional solution for the present problem, assuming the heat flow to be one-dimensional in the plate.

Assuming that the heat flow is one-dimensional in the plate, and using Eq. (21) we obtain

$$\left[\frac{\theta_f(X,0) - 1}{\lambda}\right] k = Ra^{1/3}\frac{\theta_0^{4/3}}{X^{2/3}}\hat{G}'(X,0) \quad \text{for } 0 \leqslant X \leqslant 1. \tag{34}$$

Defining the conjugate boundary temperature as $\theta_b(X) = \theta_f(X,0)$, and the average conjugate boundary temperature as $\overline{\theta}_b = \int_0^1 \theta_b(X)\,dX$ and integrating over $0 \leqslant X \leqslant 1$ on the left half of the plate, we obtain

$$\frac{k}{\lambda}(\overline{\theta}_b - 1) = 3Ra^{1/3}\theta_0^{4/3}\hat{G}'(\overline{X},0), \quad \text{where } 0 < \overline{X} < 1. \tag{35}$$

Replacing θ_0 by $\overline{\theta}_b$ and $\hat{G}'(\overline{X},0)$ by $\hat{G}'(0,0)$, Eq. (35) reduces to

$$\frac{k}{\lambda}(\overline{\theta}_b - 1) = 3Ra^{1/3}\overline{\theta}_b^{4/3}\hat{G}'(0,0). \tag{36}$$

On noting that $\hat{G}'(0,0) < 0$, we set $\gamma = -3(\lambda/k)Ra^{1/3}\hat{G}'(0,0)$ and $Z = \overline{\theta}_b^{1/3}$, so that Eq. (36) becomes

$$F_\gamma(Z) \equiv \gamma Z^4 + Z^3 - 1 = 0. \tag{37}$$

Eq. (37) has only two turning points (at $Z = -(3/4\gamma)$ and $Z = 0$), so it is clear that there can be at most three real solutions. However, since $F_\gamma(-\infty) = F_\gamma(\infty)$, there are only two real solutions possible. Having $F_\gamma(Z) > 0$ as $Z \to -\infty$ and $F_\gamma(0) = -1$, one of these solutions lies in the range $-\infty < Z < 0$, whilst the other lies in the range $0 < Z < 1$, considering the fact that $F_\gamma(1) = \gamma > 0$. Thus, the unique solution for $\overline{\theta}_b$ as a function of γ may be found using a straightforward Newton–Raphson technique.

Defining the local Nusselt number as

$$Nu(X) = -\left(\frac{\partial \theta_f}{\partial y}\right)_{y=0} \quad \text{for } 0 \leqslant X \leqslant 1$$

and the average Nusselt number as

$$\overline{Nu} = \int_0^1 Nu\,dX,$$

using the transformations (11), (15) and (20), we obtain for the local Nusselt number the following expression

$$Nu(X) = -Ra^{1/3}\frac{\theta_0^{4/3}}{X^{2/3}}\hat{G}'(X,0) \quad \text{for } 0 \leqslant X \leqslant 1. \tag{38}$$

On integrating expression (38) over the range $0 \leqslant X \leqslant 1$ and again replacing θ_0 by $\overline{\theta}_b$ and $\hat{G}'(\overline{X},0)$ by $\hat{G}'(0,0)$, we obtain for the average Nusselt number the expression

$$\overline{Nu} = -3Ra^{1/3}\bar{\theta}_b^{4/3}\hat{G}'(0,0), \tag{39}$$

where $\bar{\theta}_b$ is obtained from the solution of Eq. (37).

4. Mathematical formulation for Ra values O(1)

To obtain a solution for any Rayleigh number which is O(1), the governing equations (8a)–(8c) along with the boundary conditions (9a)–(9f) and (10a) and (10b) have to be solved numerically. The method employed is similar to that employed by Vynnycky and Kimura [19]. We first recast the equations for the fluid (8a)–(8c) into elliptical coordinates (ξ,η), with the advantage that the region near the plate, and in particular near the corners of the plate, is magnified. These coordinates are related to the Cartesian coordinates as $x = \cosh\xi\cos\eta$ and $y = \sinh\xi\sin\eta$, where $0 \leqslant \xi < \infty$ and $-\pi \leqslant \eta < \pi$. Considering the fact that the full problem is symmetrical with respect to the axis of symmetry at $x = 0$ and the fact that the elliptical coordinates are only required in the fluid region, the calculations have been performed in the region $x \geqslant 0$.

As in the boundary-layer formulation, described in Section 3, in order to provide a more accurate solution for the equations in the plate, in particular close to the edges of the plate, the transformation $\hat{\xi} = 1 - (1-x)^{2/3}$ is applied to the Eq. (8c). It should be noted that the boundary-layer calculations were performed in the region $x \leqslant 0$, which was more suitable from an analysis point of view.

In elliptical coordinates, Eqs. (8a) and (8b) become

$$\frac{\partial^2\psi}{\partial\eta^2} + \frac{\partial^2\psi}{\partial\xi^2} = Ra\left[\frac{\partial\theta_f}{\partial\eta}\cosh\xi\sin\eta - \frac{\partial\theta_f}{\partial\xi}\sinh\xi\cos\eta\right], \tag{40a}$$

$$\frac{\partial^2\theta_f}{\partial\eta^2} + \frac{\partial^2\theta_f}{\partial\xi^2} = \frac{\partial\psi}{\partial\eta}\frac{\partial\theta_f}{\partial\xi} - \frac{\partial\psi}{\partial\xi}\frac{\partial\theta_f}{\partial\eta} \tag{40b}$$

with the boundary conditions (9a)–(9f) applied for the fluid region now given by

$$\psi = 0, \qquad \theta_f = \theta_s \quad \text{on } \xi = 0 \text{ which is } y = 0,\ 0 \leqslant x \leqslant 1, \tag{41a}$$

$$\frac{\partial\theta_s}{\partial y} = \frac{1}{k\sin\eta}\frac{\partial\theta_f}{\partial\xi} \quad \text{on } \xi = 0 \text{ which is } y = 0,\ 0 \leqslant x \leqslant 1, \tag{41b}$$

$$\psi = 0, \qquad \frac{\partial\theta_f}{\partial\eta} = 0 \quad \text{on } \eta = 0 \text{ which is } y = 0,\ x \geqslant 1, \tag{41c}$$

$$\psi = 0, \qquad \frac{\partial\theta_f}{\partial\eta} = 0 \quad \text{on } \eta = \frac{\pi}{2} \text{ which is } x = 0,\ y \geqslant 0. \tag{41d}$$

In practice, the boundary conditions at large distances from the finite plate are as in Eqs. (6a) and (6b) but mathematically we have to solve the problem in a finite region of space. On the outer boundary, which computationally has to be placed at a finite distance from the heated flat plate, we have fluid flowing both into and out of the region. At the inflow boundary we have the fluid coming into the solution domain at the ambient temperature but in the situation when the fluid is leaving the solution domain we expect to have a very small normal temperature gradient on this boundary. Thus, inflow and the outflow boundary conditions are used when $u_\xi \leqslant 0$ and $u_\xi > 0$ at the outer boundary, respectively, which are given by

$$\frac{\partial\psi}{\partial\xi} \to 0, \qquad \theta_f \to 0 \quad \text{as } \xi \to \infty,\ 0 \leqslant \eta \leqslant \frac{\pi}{2} \tag{42a}$$

and

$$\frac{\partial\psi}{\partial\xi} \to 0, \qquad \frac{\partial\theta_f}{\partial\xi} \to 0 \quad \text{as } \xi \to \infty,\ 0 \leqslant \eta \leqslant \frac{\pi}{2}, \tag{42b}$$

respectively, where the expressions for the velocity components are given by

$$u_\xi = \frac{1}{M}\frac{\partial\psi}{\partial\eta}, \quad u_\eta = -\frac{1}{M}\frac{\partial\psi}{\partial\xi}, \tag{43}$$

where $M = (\cosh^2\xi\sin^2\eta + \sinh^2\xi\cos^2\eta)^{1/2}$.

Eq. (8c) for the plate region in the $(\hat{\xi}, y)$ co-ordinate system becomes

$$\frac{4}{9}(1-\hat{\xi})\frac{\partial^2\theta_s}{\partial\hat{\xi}^2} + \frac{2}{9}\frac{\partial\theta_s}{\partial\hat{\xi}} + (1-\hat{\xi})^2\frac{\partial^2\theta_s}{\partial y^2} = 0 \tag{44}$$

with the boundary conditions written for the plate region as follows:

$$\frac{\partial\theta_s}{\partial y} = \frac{1}{k\sin\eta}\frac{\partial\theta_f}{\partial\xi} \quad \text{on } y = 0,\ 0 \leqslant \hat{\xi} \leqslant 1, \tag{45a}$$

$$\theta_s = 1 \quad \text{on } y = -\lambda,\ 0 \leqslant \hat{\xi} \leqslant 1, \tag{45b}$$

$$\frac{\partial\theta_s}{\partial\hat{\xi}} = 0 \quad \text{on } \hat{\xi} = 0,\ -\lambda \leqslant y \leqslant 0, \tag{45c}$$

$$\frac{\partial\theta_s}{\partial\hat{\xi}} = 0 \quad \text{on } \hat{\xi} = 1,\ -\lambda \leqslant y \leqslant 0, \tag{45d}$$

where it should be noted that the boundary condition (9f) at $x = -1$ has been eliminated and the boundary conditions (41d) and (45c) introduced as symmetry conditions at $x = 0$.

5. Numerical techniques

Solution for $Ra \gg 1$, $0 < \theta_0 \leqslant 1$. The solution of the coupled equations for the fluid and the plate regions is obtained by an iterative method. First, the equations for the fluid region subject to their initial and boundary conditions are solved numerically by a modification of the second-order accurate finite-difference technique proposed by Merkin [22], where an initial estimate for θ_s is required at the conjugate boundary. Then the equation for the plate region, and its boundary conditions were approximated by second-order accurate finite differences over a grid used to discretise the solid plate region, which is the region $\{0 \leqslant \hat{\xi} \leqslant 1, -\lambda \leqslant y \leqslant 0\}$, and a prescribed number of iterations were processed on the resulting algebraic system of equations by the SOR iteration process, where the function $\hat{G}'$ required in the boundary conditions at $\hat{\zeta} = 0$ was obtained from the results provided by the fluid equations, and the values of $\theta_s^{\star(m)}$ were used as an estimate for the solution for $\theta_s^{\star}$, with m denoting the iteration order. The values for θ_s were obtained from the results for $\theta_s^{\star}$ and by evaluating the function $\hat{\theta}_s$, and then a combination of these values and the previous estimate for θ_s applied in the solution of the fluid equations was used instead of the estimate for θ_s for solving again the fluid equations, where the relation $\theta_s^{(m+1)} = \theta_s^{(m)} + R_o(\theta_s - \theta_s^{(m)})$ was employed, where R_o is a relaxation factor in the outer iteration procedure (it should be noted that at this point the relation $\theta_s^{\star(m+1)} = \theta_s^{\star(m)} + R_o(\theta_s - \theta_s^{\star(m)})$ was also employed). The above process of successive temporary solutions of the equations for the fluid and those for the plate was repeated until the maximum temperature difference in the plate between two successive iterations, defined by

$$\Delta\theta_s^{(m+1)} = \max_{0 \leqslant i \leqslant M, 0 \leqslant j \leqslant N} |(\theta_s)_{i,j}^{(m+1)} - (\theta_s)_{i,j}^{(m)}| \tag{46}$$

was smaller than some prescribed value ϵ, where $M+1$ and $N+1$ are the numbers of the mesh points in the $\hat{\xi}$ and the y directions, respectively, on the grid used to discretise the plate region.

In order to describe the solution procedure, the algorithm used is as follows:

(i) Set $m := 0$; Estimate $\theta_s^{(0)}$
(ii) Solve the equations which provide the initial conditions for the equations for the fluid region, to provide $\hat{F}(0,\hat{\zeta})$ and $\hat{G}(0,\hat{\zeta})$ as solution
(iii)
1. Solve the fluid equations subject to their boundary conditions using $\hat{G}(0,\hat{\zeta})$ and the values of $\theta_s^{(m)}$ given at the conjugate boundary; Provide $\hat{F}$ and $\hat{G}$ as temporary solution; Set $\hat{F}^{(m+1)} := \hat{F}$, $\hat{G}^{(m+1)} := \hat{G}$
2. Process a number of iterations in the discretised form of the equations for the plate and their boundary conditions, using the values of $\hat{G}'$ at the conjugate boundary as calculated from $\hat{G}$ and the values of $\theta_s^{\star(m)}$ as an estimate for the solution for $\theta_s^{\star}$; Provide $\theta_s^{\star}$ as temporary solution
3. Calculate θ_s, $\theta_s := \hat{\theta}_s + \theta_s^{\star}$
4. Set $\theta_s^{(m+1)} := \theta_s^{(m)} + R_o(\theta_s - \theta_s^{(m)})$; Set $\theta_s^{\star(m+1)} = \theta_s^{\star(m)} + R_o(\theta_s - \theta_s^{\star(m)})$
5. Set $m := m + 1$
6. If $\Delta\theta_s^{(m)} \geqslant \epsilon$, then go back to step (iii)(1), otherwise continue to step (iv)

(iv) Set $\theta_s := \theta_s^{(m)}$, $\hat{F} := \hat{F}^{(m)}$, $\hat{G} := \hat{G}^{(m)}$
(v) Provide solutions of the coupled equations given by $\hat{F}$, $\hat{G}$ and θ_s.

Solution for $Ra \gg 1$, $\theta_0 = 0$. The iterative method employed for the solution of the coupled equations in this case was similar to that described for $0 < \theta_0 \leqslant 1$, and we present the algorithm used as follows:

(i) Set $m := 0$; Estimate $\theta_s^{(0)}, G(X,0)$
(ii)
1. Process a number of iterations in the discretised form of the equations for the plate and their boundary conditions using the values of G at the conjugate boundary and the values of $\theta_s^{(m)}$ as an estimate for the solution for θ_s; Provide θ_s as temporary solution
2. Set $\theta_s^{(m+1)} := \theta_s^{(m)} + R_o(\theta_s - \theta_s^{(m)})$
3. Solve the equations for the fluid subject to their initial and boundary conditions using the values of $(\partial\theta_s/\partial y)^{(m+1)}$ as calculated from $\theta_s^{(m+1)}$; Provide F and G as temporary solution; Set $F^{(m+1)} := F$, $G^{(m+1)} := G$
4. Set $m := m + 1$
5. If $\Delta\theta_s^{(m)} \geqslant \epsilon$, then go back to step (ii)(1), otherwise continue to step (iii)

(iii) Set $\theta_s := \theta_s^{(m)}$, $F := F^{(m)}$, $G := G^{(m)}$
(iv) Provide solutions of the coupled equations given by F, G and θ_s.

Solution for Ra values $O(1)$. To obtain a finite-difference approximation of the equations for the fluid and the equation for the solid plate region, and their corresponding boundary conditions, the fluid region $\{0 \leqslant \eta \leqslant \pi/2,\ 0 \leqslant \xi < \xi_\infty\}$ and the solid plate region $\{0 \leqslant x \leqslant 1,\ -\lambda \leqslant y \leqslant 0\}$ were discretised, where ξ_∞ is the value set for the outer boundary in the ξ direction, and this approximation resulted in an algebraic system of equations both for the fluid and the plate regions.

The solution of the coupled plate and fluid equations is obtained by an iterative method similar to those employed for the boundary-layer solutions, namely

(i) Set $m := 0$; Estimate $\theta_s^{(0)}$, $\psi^{(0)}$, $\theta_f^{(0)}$

(ii)

1. Process a number of iterations by the SOR iterative process in the discretised form of the equations for the fluid and their boundary conditions, using the values of $\theta_s^{(m)}$ given at the conjugate boundary and the values of $\psi^{(m)}$ and $\theta_f^{(m)}$ as estimates for the solution for ψ and θ_f; Provide ψ and θ_f as temporary solution
2. Set $\psi^{(m+1)} := \psi^{(m)} + R_{o_1}(\psi - \psi^{(m)})$, $\theta_f^{(m+1)} := \theta_f^{(m)} + R_{o_1}(\theta_f - \theta_f^{(m)})$
3. Process a number of iterations by the SOR iterative process in the discretised form of the equations for the plate and their boundary conditions using the values of $(\partial\theta_f/\partial\xi)^{(m)}$ given at the conjugate boundary as calculated from $\theta_f^{(m)}$ and the values of $\theta_s^{(m)}$ as an estimate for the solution for θ_s; Provide θ_s as temporary solution
4. $\theta_s^{(m+1)} := \theta_s^{(m)} + R_{o_2}(\theta_s - \theta_s^{(m)})$
5. Set $m := m + 1$
6. If $\max\{\Delta\psi^{(m)}, \Delta\theta_f^{(m)}, \Delta\theta_s^{(m)}\} \geqslant \epsilon$, then go back to step (ii)(1), otherwise continue to step (iii)

(iii) Set $\psi := \psi^{(m)}$, $\theta_f := \theta_f^{(m)}$, $\theta_s := \theta_s^{(m)}$

(iv) Provide solutions of the elliptic equations given by ψ, θ_f and θ_s.

The maximum difference between two successive iterations of the streamfunction and the temperature is defined as in (46), with ψ and θ_f replacing θ_s, and $M + 1$ and $N + 1$ are the numbers of the mesh points in the η and the ξ directions, respectively, on the grid used to discretise the fluid region. The relaxation parameters R_{o_1} and R_{o_2} have been introduced as control parameters which restrain the diffusion from any rapid changes in the streamfunction and the fluid temperature, and in the temperature in the solid plate, respectively. The values of $\theta_s^{(m)}$ on the conjugate boundary (step (iii)(1)) are required at some mesh points of the grid used for the fluid region, however, they are given at the mesh points of the grid used for the plate region, thus linear interpolation was used between the values of $\theta_s^{(m)}(\cdot, 0)$ given at the latter mesh points in order to obtain the required value of $\theta_s^{(m)}(\cdot, 0)$. The values of $(\partial\theta_f/\partial\xi)^{(m)}(0, \cdot)$ (step (iii)(3)) were obtained in a similar way.

6. Results and discussion

Boundary-layer solution. The limiting values for the parameter σ were set to lie between 0.01 and 100. Using $\lambda = 1$ for $\sigma = 10$, the $0 < \theta_0 \leqslant 1$ formulation provided results for θ_0 close to zero, therefore the parameter ranges $0.01 \leqslant \sigma \leqslant 10$ and $5 \leqslant \sigma \leqslant 100$ were investigated by the two different formulations.

In the course of the solution for $0 < \theta_0 \leqslant 1$ when $\lambda = 1$, the procedure was found to converge rapidly for values of $\sigma \lesssim 0.2$ using no relaxation, i.e. $R_o = 1$, whilst for $\sigma \gtrsim 0.2$ the relaxation factor had to be decreased to provide convergent solutions. Thus $R_o = 0.5$, 0.1 and 0.01 were used for the parameter values $\sigma = 0.\dot{3}$, 1 and 5 and 10, respectively. When $\theta_0 = 0$ then the procedure produced convergent solutions rapidly for $\sigma \gtrsim 10$ using no relaxation ($\sigma = 10$, 20 and 100 were investigated), whilst for $\sigma = 5$ the relaxation factor had to be decreased to 0.5. When $\lambda = 0.1$, the same relaxation factors were used for $0 < \theta_0 \leqslant 1$ as when $\lambda = 1$, whilst for $\theta_0 = 0$ the solution was investigated for the parameter values $\sigma = 10$, 20 and 100, and no relaxation was required. Both for $\lambda = 1$ and 0.1 it was found that the computational time of the solution of the coupled equations increases considerably as σ increases in the $0 < \theta_0 \leqslant 1$ formulation and increases as σ decreases in the $\theta_0 = 0$ formulation.

When $0 < \theta_0 \leqslant 1$, the estimate for $\theta_s^{(0)}$ was taken to be $\theta_s^{(0)} = 1$, whilst in the case when $\theta_0 = 0$ the estimates for $\theta_s^{(0)}$ and $G(\cdot, 0)$ were taken to be $\theta_s^{(0)}(\xi, y) = -(y/\lambda)$ and $G^{(0)}(\cdot, 0) = 0$. In both situations 500 iterations were processed in the SOR iterative procedure employed for the equations in the plate region and in these equations a relaxation factor $R_p = 1.95$ was used. In the outer iterative procedure for solving the coupled equations, the looping process was repeated until $\Delta\theta_s^{(m)} < 10^{-8}$.

When $\lambda = 1$, the values of $\hat{\zeta}_\infty = 10$ for $\sigma < 1$, $\hat{\zeta}_\infty = 7.5$ for $1 \leqslant \sigma < 10$ and $\hat{\zeta}_\infty = 5$ for $\sigma = 10$ in the $0 < \theta_0 \leqslant 1$ formulation and the values of $\zeta_\infty = 17$ for $\sigma = 5$ and $\zeta_\infty = 22$ for $5 < \sigma \leqslant 100$ in the $\theta_0 = 0$ formulation were used for the location of the outer edge of the boundary-layer to obtain the results presented in this paper. It was found that an increase by approximately 30% in these values did not produce graphically distinguishable variations in the scaled non-dimensional fluid velocity $u(x, yRa^{1/3})/Ra^{2/3}$ and the temperature $\theta_f(x, yRa^{1/3})$ profiles (using $Ra = 1000$), which were calculated as a function of the scaled variable $yRa^{1/3}$. Using the same mesh locations on the horizontal $\hat{\xi}$ and X directions, then a 41×41 grid in the plate region, and 101 mesh points in the $\hat{\zeta}$ or ζ directions in the fluid region were employed, as it was found that the doubled grid sizes for both regions again produced no significant variation in the fluid velocity and temperature profiles premised. Similar calculations were performed to ensure accurate results when $\lambda = 0.1$ and the values of $\hat{\zeta}_\infty = 10$ for $\sigma < 1$, $\hat{\zeta}_\infty = 7.5$ for $1 \leqslant \sigma < 5$ and $\hat{\zeta}_\infty = 5$ for $5 \leqslant \sigma \leqslant 10$ in the $0 < \theta_0 \leqslant 1$ formulation and the value of $\zeta_\infty = 22$ for $10 \leqslant \sigma \leqslant 100$ in the $\theta_0 = 0$ formulation were set for the location of the outer edge of the boundary-layer, and a 41×11 grid and a number of 101 mesh points in the $\hat{\zeta}$ or ζ direction were used to discretise the plate and the fluid regions.

The solution of the problem in the limiting case when $\lambda = 0$ has been obtained by assuming a plate of zero thickness which has the constant non-dimensional

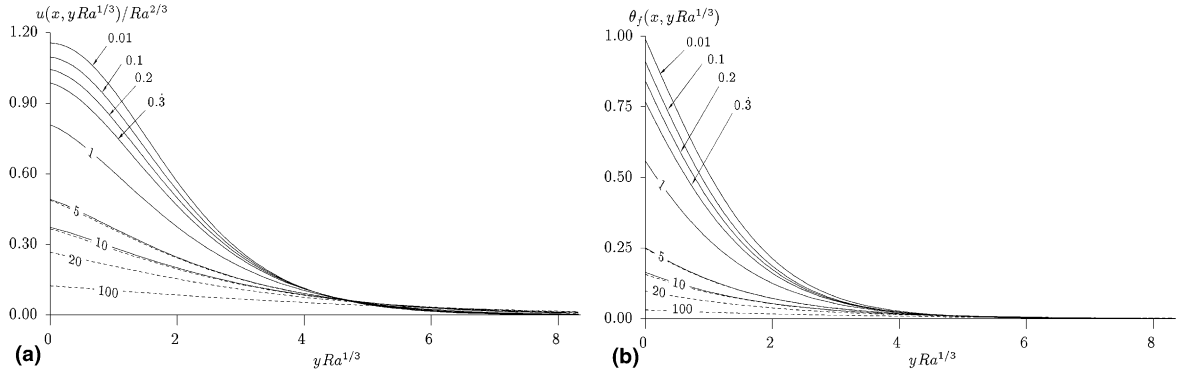

Fig. 2. (a) The fluid velocity, $u(x, yRa^{1/3})/Ra^{2/3}$, and (b) the fluid temperature profiles, $\theta_f(x, yRa^{1/3})$, as functions of $yRa^{1/3}$ for $\lambda = 1$ and $\sigma = 0.01$, 0.1, 0.2, $0.\dot{3}$, 1, 5, 10, 20 and 100 when $x = -0.2507$. The continuous and dashed lines show the results obtained by the $0 < \theta_0 \leqslant 1$ and the $\theta_0 = 0$ formulations, respectively, when $\lambda = 1$.

temperature of the unity, such that only the equations for the fluid region have to be solved. In this situation in the boundary-layer formulation there is no parameter to vary, whilst in the numerical solution the only parameter of the problem is the Rayleigh number. In the situation when the formation of a boundary-layer is assumed, the equations to be solved permit similarity solutions, see [7], whilst the numerical solution of the problem has been obtained by a modification of the method described in Section 4, when only the equations for the fluid region were considered.

Fig. 2 shows the variation of (a) the non-dimensional fluid velocity, $u(x, yRa^{1/3})/\ Ra^{2/3}$, and (b) the temperature, $\theta_f(x, yRa^{1/3})$, as a function of the scaled variable $yRa^{1/3}$ when $x = -0.2507$, for the following values of σ: 0.01, 0.1, 0.2, $0.\dot{3}$, 1, 5, 10, 20 and 100 when the parameter $\lambda = 1$. The results for $0.01 \leqslant \sigma \leqslant 10$ and $5 \leqslant \sigma \leqslant 100$, obtained by using the $0 < \theta_0 \leqslant 1$ and the $\theta_0 = 0$ formulations, are plotted by the continuous and by the dashed lines, respectively. Results for $\lambda = 0$ have been obtained when the plate is considered to have a zero thickness such that the temperature at the conjugate boundary equals unity, and these results were graphically almost indistinguishable from those obtained for $\lambda = 1$ and $\sigma = 0.01$. The results for $\sigma = 5$ and $\sigma = 10$, as obtained by using both formulations, show very good agreement both for the fluid velocity and the temperature, which validates the use of the $\theta_0 = 0$ formulation for values of $\sigma \gtrsim 5$.

In the classical problem, the formation of a boundary-layer above a heated semi-infinite thin plate maintained at a constant temperature T_c whilst the fluid temperature outside the boundary-layer is T_∞, the non-dimensional fluid velocity is assumed to be proportional to the power of the Rayleigh number $Ra^{1/3}$, which itself depends on the temperature difference $T_c - T_\infty$. Hence in the conjugate problem, we must assume that the non-dimensional fluid velocity depends directly on the non-dimensional conjugate boundary temperature. Therefore, considering that the non-dimensional conjugate boundary temperature θ_b, which is defined as $\theta_b(x) = \theta_s(x, 0)$, $-1 \leqslant x \leqslant 0$, decreases from 1 to 0 as σ increases from 0 to ∞, we expect the overall fluid velocity in the boundary-layer to decrease as σ increases, in particular in the region close to the finite plate. This is indicated by the fluid velocity profiles plotted in Fig. 2(a). In addition, since less heat is transmitted to the fluid as σ increases, it is clear that the temperature in the boundary-layer decreases, see Fig. 2(b).

However, for high values of σ the thermal conductivity of the fluid must be much higher than the thermal conductivity of the solid, so that the heat conduction effects become more pronounced in the fluid region. Therefore we expect the boundary-layer thickness to increase, and this is indicated by the fact that, see Fig. 2(a), for a larger value of σ (e.g. $\sigma = 100$) the fluid velocity decreases slower as the distance from the finite plate increases, than for a smaller value of σ (e.g. $\sigma = 1$).

Fig. 3 shows the non-dimensional conjugate boundary temperature, $\theta_b(x)$, as a function of the non-dimensional distance, x, for (a) $\lambda = 1$, and (b) $\lambda = 0.1$ and for $\sigma = 0.01$, 0.1, 0.2, $0.\dot{3}$, 1, 5, 10, 20 and 100. As for the fluid velocity and the temperature profiles from Fig. 2, in Fig. 3(a) ($\lambda = 1$) for the non-dimensional conjugate boundary temperatures there is also a good match between the results obtained by using the $0 < \theta_0 \leqslant 1$ and the $\theta_0 = 0$ formulations, as indicated by the continuous and the dashed lines, respectively, for both the parameter values $\sigma = 5$ and $\sigma = 10$. Further, the non-dimensional conjugate boundary temperature, θ_b, is close to zero in the vicinity of $x = -1$, i.e. θ_0 is close to zero for $\sigma = 5$ and for $\sigma = 10$. Therefore we can conclude that the appropriate threshold value of σ for which the $\theta_0 = 0$ formulation can be used, instead of the $0 < \theta_0 \leqslant 1$ formulation, is $\sigma = 5$.

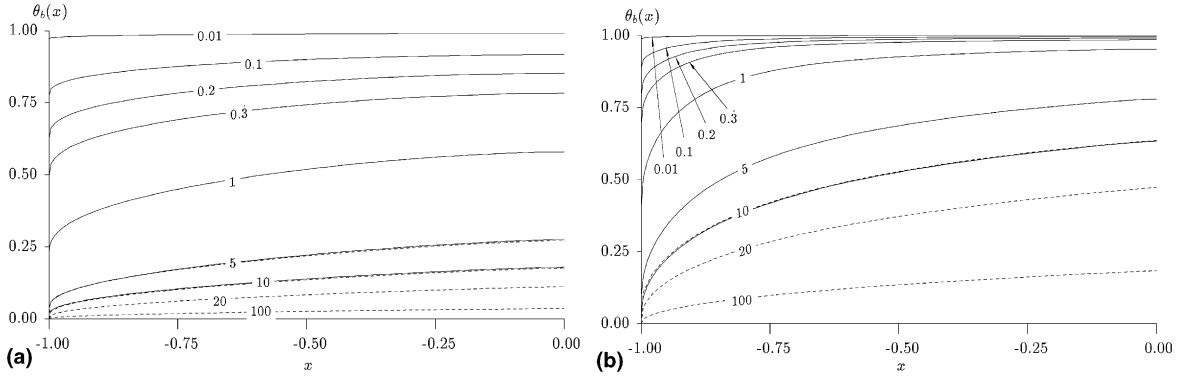

Fig. 3. The non-dimensional temperature on the conjugate boundary, $\theta_b(x)$, as a function of x, when (a) $\lambda = 1$, and (b) $\lambda = 0.1$ for $\sigma = 0.01$, 0.1, 0.2, $0.\dot{3}$, 1, 5, 10, 20 and 100. The continuous and dashed lines show the results obtained by the $0 < \theta_0 \leqslant 1$ and the $\theta_0 = 0$ formulations, respectively.

When $\lambda = 0.1$, the non-dimensional conjugate boundary temperatures obtained for the $0 < \theta_0 \leqslant 1$ and the $\theta_0 = 0$ formulations for $\sigma = 10$ are in a good agreement, and the temperature θ_0 is close to zero for this value of σ. Therefore for $\lambda = 0.1$ it is appropriate to use the $\theta_0 = 0$, rather than the $0 < \theta_0 \leqslant 1$ formulation, for values of $\sigma \gtrsim 10$. It should be noted that, in spite of the fact that the value of the parameter λ has a relatively greater change, i.e. from $\lambda = 1$ to $\lambda = 0.1$, the threshold value for σ for which the $\theta_0 = 0$ formulation may be used, rather than the $0 < \theta_0 \leqslant 1$ formulation, is not very sensitive to this change. Further, the non-dimensional conjugate boundary temperatures obtained for $\lambda = 0.1$ were found to be higher than those obtained for $\lambda = 1$, for a fixed value of the parameter σ, and this indicates that the effect of a change in the plate aspect ratio λ is similar to the effect of a change in the parameter σ, when controlling the heat diffusion through the fluid. Therefore decreasing λ and keeping σ fixed has the same effect as decreasing σ and keeping λ fixed, i.e. more heat is conducted to the fluid.

In addition, Fig. 3 indicates that for the larger plate aspect ratio, $\lambda = 1$, the temperatures at the fluid–solid interface are much closer to being linear in x than for the situation $\lambda = 0.1$. In particular, although these temperatures increase rapidly, both for $\lambda = 1$ and $\lambda = 0.1$, close to the left edge of the finite plate, i.e. close to $x = -1$, the rate of increase is much greater for $\lambda = 0.1$. This demonstrates that the decrease of the plate aspect ratio has the effect of smoothing the rapid changes in the temperature at the fluid–solid interface.

Approximate one-dimensional solution. The average conjugate boundary temperature, $\overline{\theta}_b$, plotted in Fig. 4, can be obtained by solving Eq. (37), and they may be collapsed onto one curve, regardless of the values of *Ra*, *k* and λ, and depend only on the value of the parameter γ. In turn, the results for $\overline{Nu}$ can be obtained from the expression (39) and they depend on γ and *Ra*. Despite the approximate nature of this analytical approach, it provides an engineering perspective from which it is easy to obtain approximate results for $\overline{\theta}_b$ and $\overline{Nu}$, which, as shown later in this section, compare extremely well with both the boundary-layer solutions and the full numerical solutions. It should be noted that on solving the equations which provide the initial conditions for the equations for the fluid region, it was found that $\hat{G}'(0,0) = -0.430031$, which compares well with the results obtained by Cheng and Chang [7], who found that $\hat{G}'(0,0) = -0.4299$.

Numerical solution. Whilst in the boundary-layer formulation there are two parameters, namely σ and λ, in the full formulation the number of the parameters is

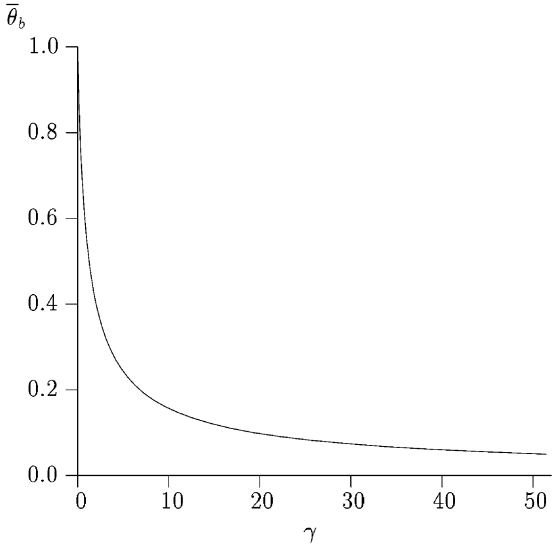

Fig. 4. The average conjugate boundary temperature, $\overline{\theta}_b$, as a function of the parameter γ.

three, namely, Ra, k and λ. The calculations for the numerical solution have been performed in the fluid region $\{0 \leqslant \xi < \infty,\ 0 \leqslant \eta \leqslant (\pi/2)\}$ and in the finite plate region $\{0 \leqslant x \leqslant 1,\ -\lambda \leqslant y \leqslant 0\}$, but all the solutions are presented in the regions in the left side of the axis of symmetry, $x = 0$, i.e. $\{0 \leqslant \xi < \infty,\ (\pi/2) \leqslant \eta \leqslant \pi\}$ and $\{-1 \leqslant x \leqslant 0,\ -\lambda \leqslant y \leqslant 0\}$, in order to compare them with the solutions obtained by using the boundary-layer formulation.

When solving Eqs. (40a) and (40b) and (41a)–(41d) in the fluid region, an appropriate location for infinity had to be chosen in order to take account of the overall heat-transfer characteristics. As a representative value for the location of infinity, we have chosen its position in the x direction, x_∞, which is related to the location of the infinity in the ξ direction, ξ_∞, by the relation $x_\infty = \cosh(\xi_\infty)$. The appropriate location of the infinity boundary was investigated for different values of the Rayleigh number in the range of $1 \leqslant Ra \leqslant 100$ and for a given value of Ra the value chosen for the location of infinity proved to be very important when calculating the overall heat-transfer. In order to achieve a numerical solution which was independent of the location of the infinity boundary condition, the mean Nusselt number, $\overline{Nu}$, and the mean fluid velocity, $\overline{u}_b$, along the conjugate boundary, were calculated for different values of x_∞. First, the value of x_∞ was set to be $x_\infty \approx 2.5$, then this value was doubled, and this procedure was repeated until the results found for both $\overline{Nu}$ and $\overline{u}_b$ agreed within about 1% for two successive values of x_∞.

In order to find a solution which is independent of the mesh size, then some arbitrary grid size was chosen and calculations were performed with this grid size and with the doubled grid size and again, if the values calculated for $\overline{Nu}$ and $\overline{u}_b$ agreed within about 1% then the grid was considered appropriate to provide an accurate solution. In these calculations the value of the ratio of the thermal conductivities of the solid and the fluid, k, was taken to be $k = 1000$ and $k = 1$ which were considered as limiting values for the parameter k.

Although the quantities $\overline{Nu}$ and $\overline{u}_b$ show characteristics of the heat transfer and of the flow only at the conjugate boundary, we considered that if the results for these quantities obtained by using different parameters of the problem are accurate, i.e. they agree within about 1%, then the solutions obtained by using the latter parameters will provide accurate results for all the domain inspected and this is because all the heat transfer and fluid flow characteristics depend strongly on the processes which take place at the conjugate boundary, i.e. on the heat conducted through the conjugate boundary.

Thus it was found that for $\lambda = 1$ the value pairs of $(x_\infty,\ M_\eta \times N_\xi + M_{\hat{\xi}} \times N_y) = (160.110, 80 \times 120 + 80 \times 40)$, $(20.035, 80 \times 120 + 80 \times 40)$ and $(2.577, 80 \times 80 + 80 \times 40)$, for the location of the infinity boundary and for the grid sizes used for $Ra = 1$, $Ra = 10$ and $Ra \geqslant 100$, respectively, are appropriate both when $k = 1$ and $k = 1000$. Hence for any $1 \leqslant k \leqslant 1000$ these numerical parameter values were used to obtain all the results presented in this paper for $Ra = 1$, $Ra = 10$ and $Ra \geqslant 100$. The results presented for $\lambda = 0.1$ were obtained by using the same numerical parameters, except that $N_y = 10$.

The numerical parameters presented indicate that at the lower Rayleigh numbers the location of the infinity boundary needs to be set very far from the plate, whilst for higher Rayleigh numbers it is possible to obtain an accurate solution using lower values for the location of the infinity boundary. This is due to the fact that at lower Rayleigh numbers the convective motion is slower, and the conduction effects are more pronounced. This causes the heat to be radially diffused far from the plate through infinity, whilst at high Rayleigh numbers a convective boundary-layer develops, and significant heat transfer takes place in the vicinity of the finite plate in this boundary-layer region. The values of $\overline{Nu}$ and $\overline{u}_b$ increase as Ra increases, and this also indicates the level of the intensification of the heat transfer processes close to the plate.

Various relaxation parameters were used in the SOR iterative procedures employed for the discretised form of the equations. Thus the relaxation parameters $(R_{f_1}, R_{f_2}, R_p) = (1.8, 1.95, 1.95)$, $(0.8, 0.8, 1.95)$, $(0.5, 0.8, 1.95)$ and $(0.3, 0.3, 1)$ for $k = 1000$ and $(R_{f_1}, R_{f_2}, R_p) = (1.95, 1.95, 1.3)$, $(1.8, 0.6, 1)$, $(1.8, 0.4, 0.8)$ and $(1.8, 0.4, 0.8)$ for $k = 1$ were used for $Ra = 1$, 10, 100 and 1000, respectively, where R_{f_1}, R_{f_2} and R_p are the relaxation parameters for the Eqs. (40a), (40b) and (44), respectively, and they were used as normative values when obtaining results for other values of the parameters Ra and k.

The relaxation factors R_{o_1} and R_{o_2}, which are employed in the algorithm used for the numerical solution of the coupled equations, were found to provide convergent solutions when using $R_{o_1} = R_{o_2} = 1$, i.e. there is no relaxation, for all the Rayleigh numbers investigated. However, in the solution of the coupled equations when using the boundary-layer formulation, the relaxation factors R_o which are introduced in the algorithms employed for the $0 < \theta_0 \leqslant 1$ and $\theta_0 = 0$ formulations, had to be decreased to smaller values than the unity when the parameter σ was greater than a certain value. It should be noted that the relaxation factor R_o used in the boundary-layer formulation has a similar effect as the relaxation factor R_{o_2} which is used in the numerical solution of the coupled equations, namely the effect of controlling the heat diffused from the finite plate to the fluid region.

The estimates required in the algorithm employed for the numerical solution were taken to be $\theta_s^{(0)} = 1$, $\psi^{(0)} = 0$ and $\theta_f^{(0)} = 0$, and both in the equations for the fluid region and in the heat conduction equation in the finite plate only one iteration was processed in order to speed up the information being diffused between the two re-

Table 1
The average conjugate boundary temperature, $\overline{\theta}_b$, the average Nusselt number on the conjugate boundary, $\overline{Nu}$, obtained for the plate aspect ratios $\lambda = 1$ and $\lambda = 0.1$

	$\sigma = 0.1$		$\sigma = 1$		$\sigma = 10$	
	$\overline{\theta}_b$	$\overline{Nu}$	$\overline{\theta}_b$	$\overline{Nu}$	$\overline{\theta}_b$	$\overline{Nu}$
$\lambda = 1$						
1D	0.8896	11.0381	0.4949	5.0507	0.1321	0.8679
B-l	0.8888	10.9093	0.4905	5.0219	0.1270	0.8685
Num	0.8894	10.4548	0.4946	4.9756	0.1262	0.8687
$\lambda = 0.1$						
1D	0.9873	12.6832	0.8896	11.0381	0.4949	5.0507
B-l	0.9869	11.8304	0.8897	10.6197	0.4884	5.0854
Num	0.9873	12.1218	0.8913	10.6752	0.4858	5.1270

When obtained by using the boundary-layer and the approximate one-dimensional solutions, then $\sigma = 0.1$, 1 and 10. When obtained by using the numerical solution, then $Ra = 1000$ and $k = 100$, 10 and 1.

gions. Further, the error ϵ used in the stopping criterion from the outer loop of the algorithm was required to be set as small as $\epsilon = 10^{-8}$ in order to provide an accurate solution for all the parameter values investigated.

Comparisons. Table 1 presents results for the average conjugate boundary temperature, $\overline{\theta}_b$, and for the average Nusselt number, $\overline{Nu}$, on the conjugate boundary, results calculated from the solution obtained by using the boundary-layer formulation and from the approximate one-dimensional solution for the values of the parameter $\sigma = 0.1, 1$ and 10, and for the plate aspect ratios $\lambda = 1$ and 0.1, and calculated from the solution obtained by using the numerical solution for the corresponding values of k when $Ra = 1000$, i.e. for $k = 100$, 10 and 1. It is evident in Table 1 that there is good agreement between the results obtained by using all the three solution methods for the parameter values presented, both for $\overline{\theta}_b$ and $\overline{Nu}$. In particular, the results obtained for $\overline{\theta}_b$ and $\overline{Nu}$ by the approximate one-dimensional solution compare very well with the results obtained by using the boundary-layer and the numerical solutions despite its approximate approach, and it is important to mention that for $\lambda = 0.1$, the agreement for $\overline{\theta}_b$ and $\overline{Nu}$ is still very good, although we expect better agreement for $\lambda = 1$ than for $\lambda = 0.1$. This expectation is due to the fact that the conjugate boundary temperatures obtained by using the boundary-layer solution are much closer to being linear in x for $\lambda = 1$ than for $\lambda = 0.1$, see Fig. 3.

Fig. 5 shows the (i) streamlines and (ii) isotherms as obtained from the numerical solution. The results are calculated for the Rayleigh numbers $Ra = 1$ in Figs. 5(a) and (b), and $Ra = 1000$ in Figs. 5(c) and (d), and the ratios of the thermal conductivities in the solid and in the fluid are $k = 1$ in Figs. 5(a) and (c), and $k = 100$ in Fig. 5(b) and (d). When the Rayleigh number is relatively small, i.e. $Ra = 1$ in our case (Figs. 5(a) and (b)), the streamlines show a weak entrainment of the fluid, which is observed by the small values of the streamfunction. However, for $k = 100$ the fluid movement is more intense than for $k = 1$, as indicated by the closer contour spacings. The effect of the difference in the values of k is also indicated by the isotherms, which show a much greater decrease of the temperature for $k = 100$ than for $k = 1$. In addition, the isotherms indicate the significance of the conduction as opposed to the convection in the fluid as observed by the uniform temperature distribution in the fluid region.

As opposed to the situation when the Rayleigh number is small, when the Rayleigh number is relatively large, i.e. $Ra = 1000$ in our case (Fig. 5(c) and (d)), the streamlines show a much stronger entrainment of the fluid, and this is observed by the relatively large values of the streamfunction that occur. The streamline plots show that the fluid flow is directed from the outer regions of the fluid to the vicinity of the finite plate, where they are approximately horizontal above the finite plate before they become almost vertical near the central vertical plane of the fluid region. This indicates that for high Rayleigh numbers a boundary-layer develops in the vicinity of the finite plate, and a vertical jet-like flow is present in the central region of the fluid. In turn, the isotherm plots show that for $k = 1$ the non-dimensional temperature at the conjugate boundary is approximately 0.1, i.e. almost all of the heat is enclosed in the finite plate, whilst for $k = 100$ this temperature is approximately 0.9, i.e. most of the heat is diffused to the fluid.

We conclude that the effect of the ratio of the thermal conductivities, k, is more important in the case of large Rayleigh numbers than for small Rayleigh numbers, as regards the amount of the heat conducted to the fluid region. This is most noticeable in the isotherms, but it is also seen by the much faster decrease of the streamfunction in the fluid region. Based on these observations, the formation of a boundary-layer is more clearly observed for $k = 100$ than for $k = 1$.

Fig. 6 shows the (i) streamline and (ii) isotherm plots when $\lambda = 1$, plots of the results obtained from the numerical solution and by the boundary-layer solution. The results have been obtained using the numerical solution for (a) $Ra = 1000$ and $k = 100$, (b) for $Ra = 1000$ and $k = 10$, and (c) for $Ra = 1000$ and $k = 1$, and from the boundary-layer solution for the corresponding values of σ, i.e. for $\sigma = 0.1$, 1 and 10. The results obtained by using the numerical solution and by the boundary-layer solution are plotted by the continuous lines and by the dashed lines, respectively.

The streamlines for the numerical solution indicate that after the fluid is entrained from outside the boundary-layer then it accelerates in the boundary-layer and the flow has a jet-like structure near the central vertical plane, whilst the streamline plots for the boundary-layer solution show a flow structure which is approximately parallel to the finite plate. This difference in the flow structure is due to the fact that the numerical solution takes account of the symmetry at the central vertical plane, whilst in the boundary-layer solution the boundary-layer developed in the left side of the central

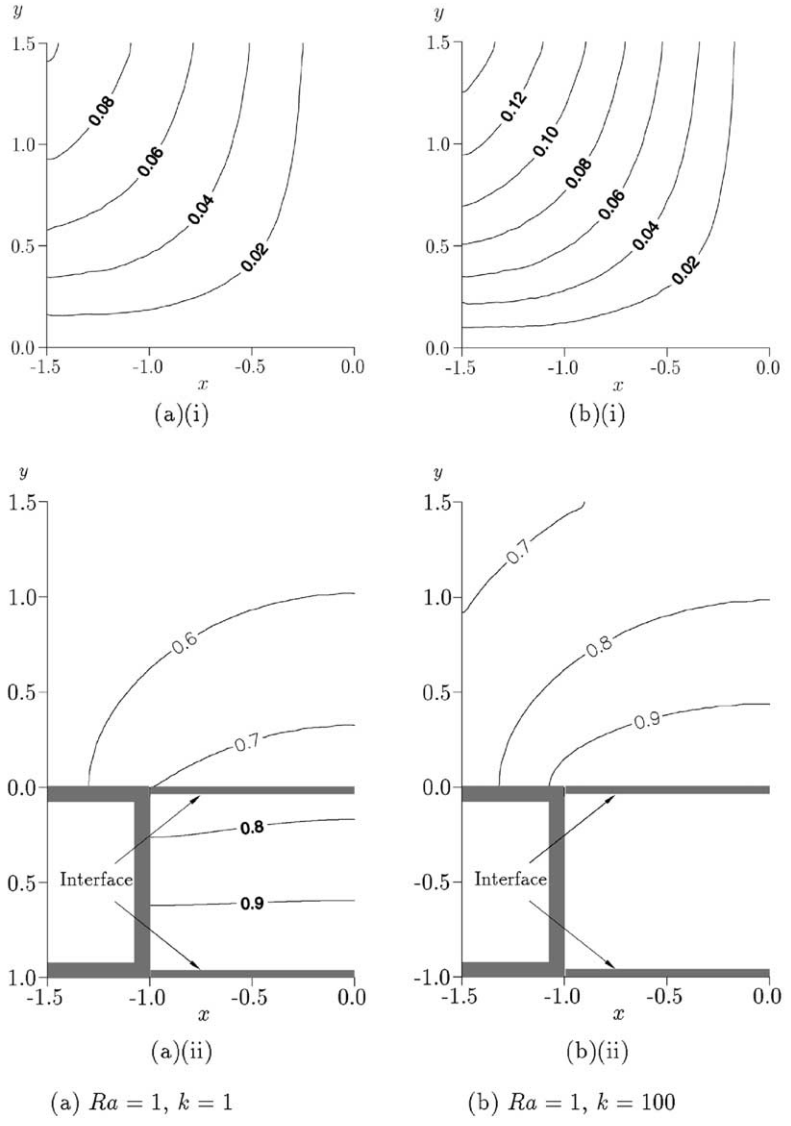

Fig. 5. (i) Streamlines and (ii) isotherms, as calculated from the numerical solution for $Ra = 1$ and 1000, $k = 1$ and 100 and $\lambda = 1$.

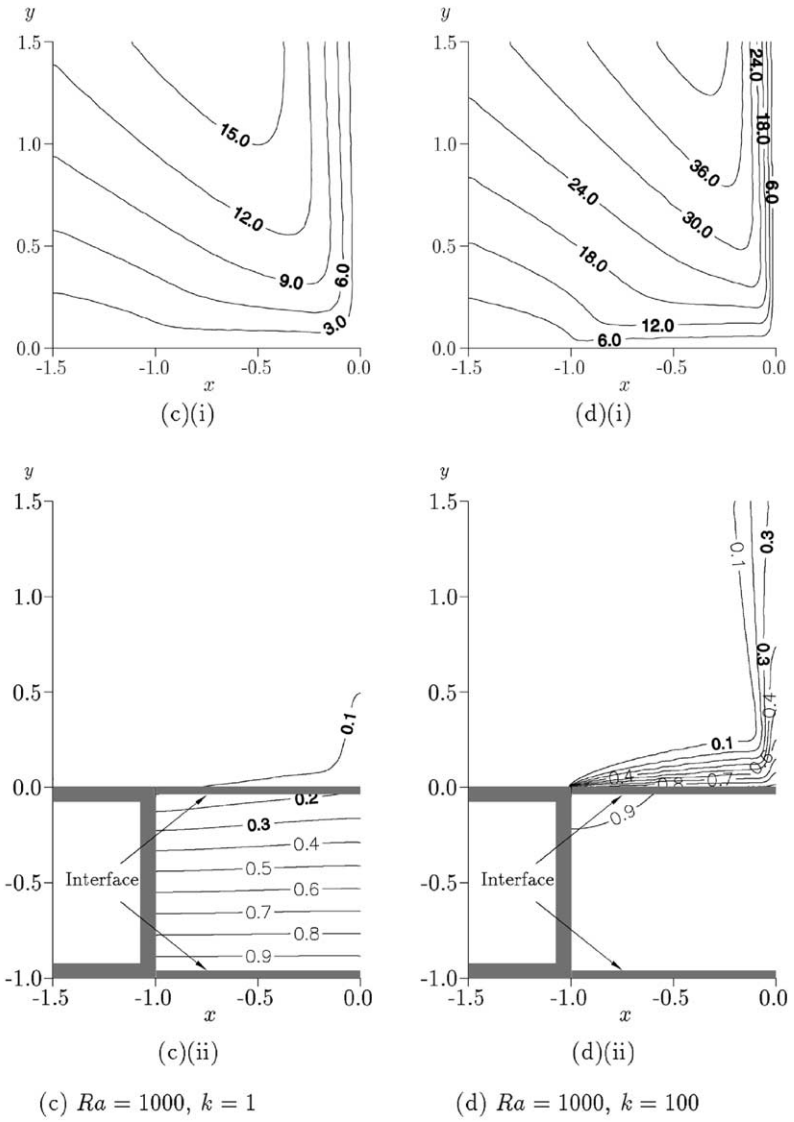

Fig. 5 (*continued*)

vertical plane does not take account of the boundary-layer present on the right side of the central vertical plane, which opposes the flow.

In the finite plate region the results for the temperature fields are in a good agreement, as indicated by the isotherms. In the fluid region the boundary-layer solution is a good approximation for the numerical solution in the range $-1 \lesssim x \lesssim -0.1$, both for the flow and for the temperature fields, especially in the region close to the finite plate, whilst in the range $-0.1 \lesssim x \leqslant 0$, near the central vertical plane, there can be no agreement since two quite different flow regimes are assumed by the two different formulations.

The (a), (b) and (c) in Fig. 6, for $k = 100$, 10 and 1, respectively, indicate that for $-1 \lesssim x \lesssim -0.1$ the agreement between the results both for the flow and the temperature fields in the fluid region deteriorates with decreasing values of k, and this is due to the less intense heating of the fluid by the finite plate when k decreases, i.e. the boundary-layer assumption becomes less valid. However, in the region close to the finite plate there is good agreement for all three values of k.

The assumption made in the solution of the boundary-layer equations that the flow is at rest on the left side of the finite plate for $x \leqslant -1$, has been shown to be appropriate, since the boundary-layer and the numerical

solutions obtained for $Ra = 1000$, i.e. for a boundary-layer regime, are in a good agreement close to $x = -1$.

Fig. 7 shows (i) the conjugate temperature $\theta_b(x)$, and (ii) the local Nusselt number $Nu(x)$, as functions of x, when $\lambda = 1$ for (a) $\sigma = 0.1$, (b) $\sigma = 1$ and (c) $\sigma = 10$, obtained from the boundary-layer and the numerical solutions. The numerical results were obtained for the Rayleigh numbers $Ra = 300$, 600 and 1000 and for the corresponding values of k ($k = 66.9433$, 84.3433 and 100 when $\sigma = 0.1$).

These plots show that as the ratio of the thermal conductivities of the finite plate and the fluid, k, decreases, and the Rayleigh number remains the same, i.e. the value of σ decreases in the boundary-layer solution, then the agreement between the numerical and the boundary-layer results reduces both for the temperature and the Nusselt number at the conjugate boundary. The agreement between the results for $\theta_b(x)$ and $Nu(x)$ from the boundary-layer solution and the numerical solution for $Ra = 1000$ is very good for $\sigma = 0.1$ (see Fig. 7(a)) in all the range $-1 \leqslant x \leqslant 0$, for $\sigma = 1$ (see Fig. 7(b)) the matching is good up to about $x = -0.07$, whilst for $\sigma = 10$ (see Fig. 7(c)) a very good match can be considered only up to about $x = -0.5$, but a reasonably good match up to about $x = -0.1$ is observed.

As observed in Table 1, there is a good agreement for $\overline{\theta}_b$ and $\overline{Nu}$ for $\sigma = 0.1$, 1 and 10 ($\lambda = 1$), and this is also confirmed by Fig. 7. Although the results for θ_b and Nu plotted for $\sigma = 10$ (see Fig. 7(c)) have a relatively large variation near $x = 0$ when calculated by the numerical solution when $Ra = 1000$, compared to the case when they are calculated by the boundary-layer solution, the good agreement for $\overline{\theta}_b$ and $\overline{Nu}$ for $\sigma = 10$ is due to the averaging that takes place for $\overline{\theta}_b$ and $\overline{Nu}$ in the range $-1 \leqslant x \leqslant 0$.

In all three situations presented, i.e. for $\sigma = 0.1$, 1 and 10, the agreement is better for $Ra = 1000$ than for $Ra = 300$ and $Ra = 600$, but even for the latter cases the agreement appears to be good. Thus the boundary-layer formulation may be used, with confidence, over a wide range of values of Ra, particularly for $Ra \geqslant 300$.

Fig. 8 shows the (i) streamline and (ii) isotherm plots of the results obtained for $\lambda = 0$ by the numerical solution when $Ra = 1000$ and by the boundary-layer solution using $Ra = 1000$ when scaling the variable y, and they are plotted by the continuous lines and by the dashed lines, respectively.

As discussed earlier in this section, (a), (b) and (c) in Fig. 6 indicate that for $-1 \lesssim x \lesssim -0.1$ the agreement between the results obtained both for the flow and the temperature fields in the fluid region improves with increasing values of k for the plate aspect ratio, $\lambda = 1$. This is due to the more intense heating of the fluid by the finite plate with increasing values of k, which indirectly implies increasing values of the temperature of the conjugate boundary. However, in the limiting case of $\lambda = 0$ we assume that the conjugate boundary has the temperature of unity, therefore we expect that in this case the agreement between the results obtained by using the boundary-layer and the numerical solutions improves even more, and this is clear from the plots shown in Fig. 8.

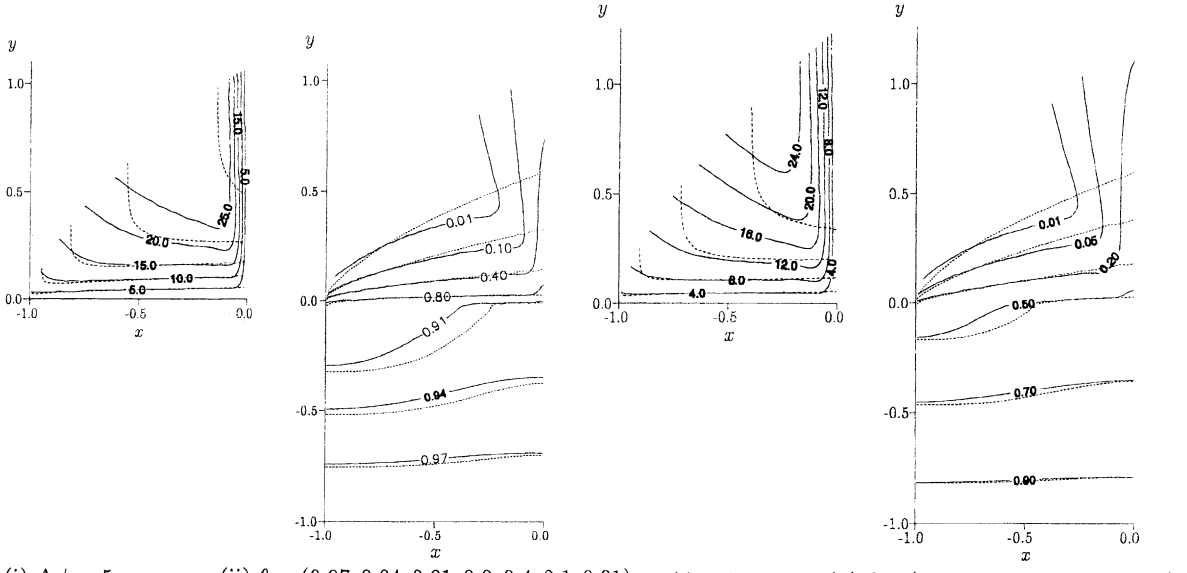

(i) $\Delta\psi = 5$ (ii) $\theta = (0.97; 0.94; 0.91; 0.8; 0.4; 0.1; 0.01)$ (i) $\Delta\psi = 4$ (ii) $\theta = (0.9; 0.7; 0.5; 0.2; 0.05; 0.01)$

(a) $Ra = 1000$, $k = 100$ ($\sigma = 0.1$) **(b)** $Ra = 1000$, $k = 10$ ($\sigma = 1$)

Fig. 6. (i) Streamlines, and (ii) isotherms, calculated for $\lambda = 1$. The continuous and dashed lines show the results obtained from the numerical solutions and the boundary-layer solutions, respectively.

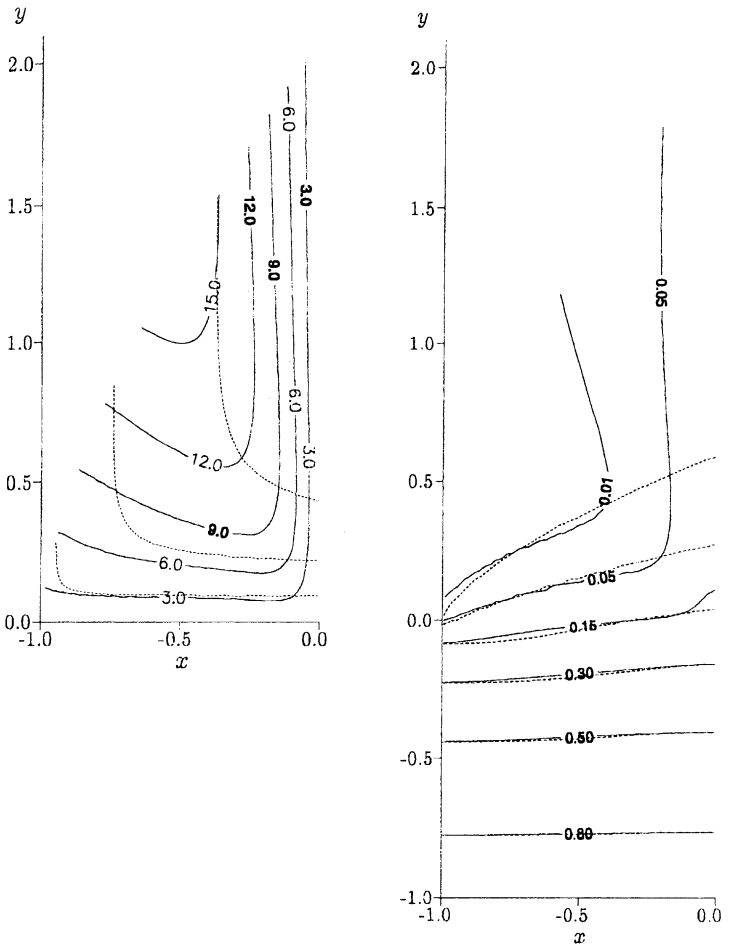

(i) $\Delta\psi = 3$ (ii) $\theta = (0.8; 0.5; 0.3; 0.15; 0.05; 0.01)$

(c) $Ra = 1000,\ k = 1\ (\sigma = 10)$

Fig. 6 (*continued*)

7. Concluding remarks

In this paper, three methods have been developed in order to investigate the phenomenon of free convection in a porous medium above a heated finite plate in the conjugate case when the Rayleigh number is high and a boundary-layer flow develops above the finite plate. These three methods, namely a boundary-layer solution, an approximate solution which assumes that the heat conduction in the plate is one-dimensional, and a numerical solution of the full equations in a finite region of space, provided results which were in very good agreement. A detailed examination of the conjugate effects was given by the boundary-layer and the numerical solutions, showing that the thickness of the finite plate, λ, and the so-called conjugate parameter, k, both play an important role in the heat-transfer processes in the boundary-layer.

It is important to investigate the phenomenon of convection for Ra values O(1), and the numerical solution proved to provide a very effective solution model for this problem. In this solution process the equations for the fluid and the plate regions are not solved separately at every step of the overall iteration, as is common in conjugate problems, instead the solution process evolves synchronically in the fluid and the plate regions, furnishing results much more rapidly. Further, the representation of the fluid region in elliptical coordinates provides a very effective survey method, which naturally magnifies the region close to the plate. In addition, the use of inflow and outflow boundary conditions employed at the outer boundary allows a considerable

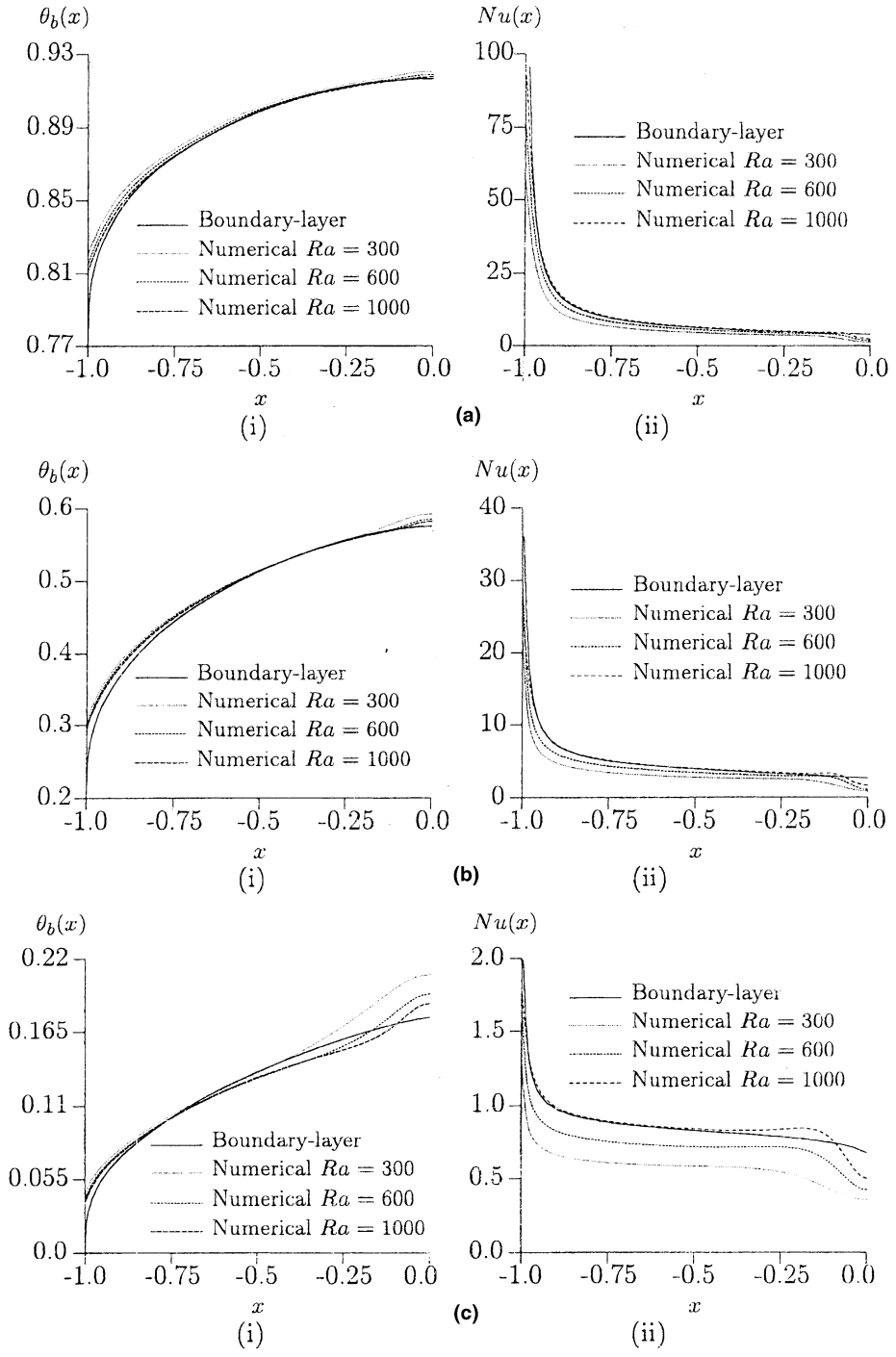

Fig. 7. (i) The conjugate boundary temperature, $\theta_b(x)$, and (ii) the local Nusselt number $Nu(x)$, as functions of the distance along the finite plate, x, for (a) $\sigma = 0.1$, (b) $\sigma = 1$, and (c) $\sigma = 10$ obtained by the boundary-layer and the numerical solution for the Rayleigh numbers $Ra = 300$, 600 and 1000.

reduction in the fluid region investigated for high Rayleigh numbers, which is extremely important since in this case a very refined mesh is required close to the plate.

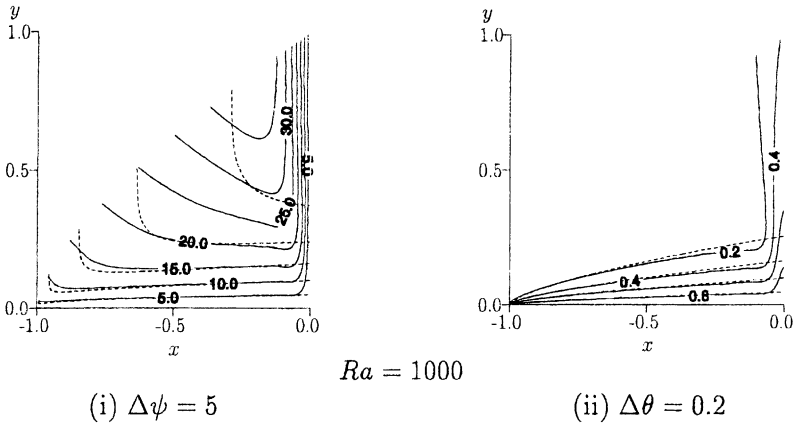

Fig. 8. (i) Streamlines, and (ii) isotherms, calculated for $Ra = 1000$. The continuous and dashed lines show the results obtained by using the numerical and the boundary-layer solutions, respectively.

Acknowledgements

Two of the authors, Professors D.B. Ingham and I. Pop, gratefully acknowledge The Royal Society for supporting some of the research described in this paper.

References

[1] A. Nakayama, PC-aided Numerical Heat Transfer and Convective Flow, CRC Press, Tokyo, 1995.
[2] D.A. Nield, A. Bejan, Convection in Porous Media, Springer, New York, 1999.
[3] D.B. Ingham, I. Pop (Eds.), Transport Phenomena in Porous Media, Pergamon, Oxford, 1998.
[4] D.B. Ingham, I. Pop (Eds.), Transport Phenomena in Porous Media, vol. 2, Pergamon, Oxford, 2001.
[5] K. Vafai (Ed.), Handbook of Porous Media, Marcel Dekker, New York, 2000.
[6] I. Pop, D.B. Ingham, Convective Heat Transfer: Mathematical and Computational Modelling of Pergamon, Pergamon, Oxford, 2001.
[7] P. Cheng, I.D. Chang, Buoyancy induced flows in a saturated porous medium adjacent to impermeable horizontal surfaces, Int. J. Heat Mass Transfer 19 (1976) 1267–1272.
[8] J.H. Merkin, G. Zhang, On the similarity solutions for free convection in a saturated porous medium adjacent to impermeable horizontal surfaces, Wärme- Stoffübertr 25 (1990) 179–184.
[9] F.I. Higuera, P.D. Weidman, Natural convection beneath a downward facing heated plate in a porous medium, Eur. J. Mech. B/Fluids 14 (1995) 29–40.
[10] M.A. Chandhary, J.H. Merkin, I. Pop, Natural convection from a horizontal permeable surface in a porous medium–numerical and asymptotic solution, Transp. Porous Media 22 (1996) 327–344.
[11] S. Kimura, A. Bejan, I. Pop, Natural convection near a cold plate facing upward in a porous medium, J. Heat Transfer 107 (1985) 819–825.
[12] M. Vynnycky, S. Kimura, Conjugate free convection due to a vertical plate in a porous medium, Int. J. Heat Mass Transfer 37 (1994) 229–236.
[13] M. Vynnycky, S. Kimura, Transient conjugate free convection due to a vertical plate in a porous medium, Int. J. Heat Mass Transfer 38 (1995) 219–231.
[14] D. Lesnic, D.B. Ingham, I. Pop, Conjugate free convection from a horizontal surface in a porous medium, Z. Angew. Math. Mech. 75 (1995) 715–722.
[15] I. Pop, J.H. Merkin, Conjugate free convection on a vertical surface in a saturated porous medium, Fluid Dyn. Res. 16 (1995) 71–86.
[16] F.I. Higuera, Conjugate natural convection heat transfer between two porous media separated by a horizontal wall, Int. J. Heat Mass Transfer 40 (1997) 3157–3161.
[17] F.I. Higuera, I. Pop, Conjugate natural convection heat transfer between two porous media separated by a vertical wall, Int. J. Heat Mass Transfer 40 (1997) 123–129.
[18] S. Kimura, T. Kiwata, A. Okajima, I. Pop, Conjugate natural convection in porous media, Adv. Water Resour. 20 (1997) 111–126.
[19] M. Vynnycky, S. Kimura, Conjugate free convection due to a heated vertical plate, Int. J. Heat Mass Transfer 39 (1996) 1067–1080.
[20] M. Vynnycky, I. Pop, Mixed convection due to a finite horizontal flat plate embedded in a porous medium, J. Fluid Mech. 351 (1997) 359–378.
[21] M. Vynnycky, S. Kimura, K. Kanev, I. Pop, Forced convection heat transfer from a flat plate: the conjugate problem, Int. J. Heat Mass Transfer 41 (1998) 45–59.
[22] J.H. Merkin, Free convection boundary layer on an isothermal horizontal cylinder: ASME-AICHE National Heat Transfer Conf., 76-HT-16, St. Louis, USA, 1976.